

Wrinkles in the *Gaia* data unveil a dynamically young and perturbed Milky Way disk

T. Antoja^{1,*}, A. Helmi², M. Romero-Gómez¹, D. Katz³, C. Babusiaux⁴, R. Drimmel⁵, D. W. Evans⁶, F. Figueras¹, E. Poggio^{5,7}, C. Reylé⁸, A.C. Robin⁸, G. Seabroke⁹, and C. Soubiran¹⁰

¹Institut de Ciències del Cosmos, Universitat de Barcelona (IEEC-UB), Martí i Franquès 1, E-08028 Barcelona, Spain

²Kapteyn Astronomical Institute, University of Groningen, Landleven 12, 9747 AD Groningen, The Netherlands

³GEPI, Observatoire de Paris, Université PSL, CNRS, 5 Place Jules Janssen, 92190 Meudon, France

⁴Univ. Grenoble Alpes, CNRS, IPAG, 38000 Grenoble, France

⁵INAF - Osservatorio Astrofisico di Torino, via Osservatorio 20, 10025 Pino Torinese (TO), Italy

⁶Institute of Astronomy, University of Cambridge, Madingley Road, Cambridge CB3 0HA, UK.

⁷Università di Torino, Dipartimento di Fisica, via Pietro Giuria 1, 10125 Torino, Italy

⁸Institut UTINAM, CNRS UMR6213, Univ. Bourgogne Franche-Comté, OSU THETA Franche-Comté Bourgogne, Observatoire de Besançon, BP 1615, 25010 Besançon Cedex, France.

⁹Mullard Space Science Laboratory, University College London, Holmbury St Mary, Dorking, Surrey RH5 6NT, United Kingdom

¹⁰Laboratoire d'astrophysique de Bordeaux, Univ. Bordeaux, CNRS, B18N, allée Geoffroy Saint-Hilaire, 33615 Pessac, France

*tantoja@fqa.ub.edu

ABSTRACT

Most of the stars in our Galaxy including our Sun, move in a disk-like component¹ and give the Milky Way its characteristic appearance on the night sky. As in all fields in science, motions can be used to reveal the underlying forces, and in the case of disk stars they provide important diagnostics on the structure and history of the Galaxy². But because of the challenges involved in measuring stellar motions, samples have so far remained limited in their number of stars, precision and spatial extent. This has changed dramatically with the second Data Release of the *Gaia* mission which has just become available³. Here we report that the phase space distribution of stars in the disk of the Milky Way is full of substructure with a variety of morphologies, most of which have never been observed before. This includes shapes such as arches and shells in velocity space, and snail shells and ridges when spatial and velocity coordinates are combined. The nature of these substructures implies that the disk is phase mixing from an out of equilibrium state, and that the Galactic bar and/or spiral structure are strongly affecting the orbits of disk stars. Our analysis of the features leads us to infer that the disk was perturbed between 300 and 900 Myr ago, which matches current estimations of the previous pericentric passage of the Sagittarius dwarf galaxy. The *Gaia* data challenge the most basic premise of stellar dynamics of dynamical equilibrium, and show that modelling the Galactic disk as a time-independent axisymmetric component is definitely incorrect. These findings mark the start of a new era when, by modelling the richness of phase space substructures, we can determine the gravitational potential of the Galaxy, its time evolution and the characteristics of the perturbers that have most influenced our home in the Universe.

Main

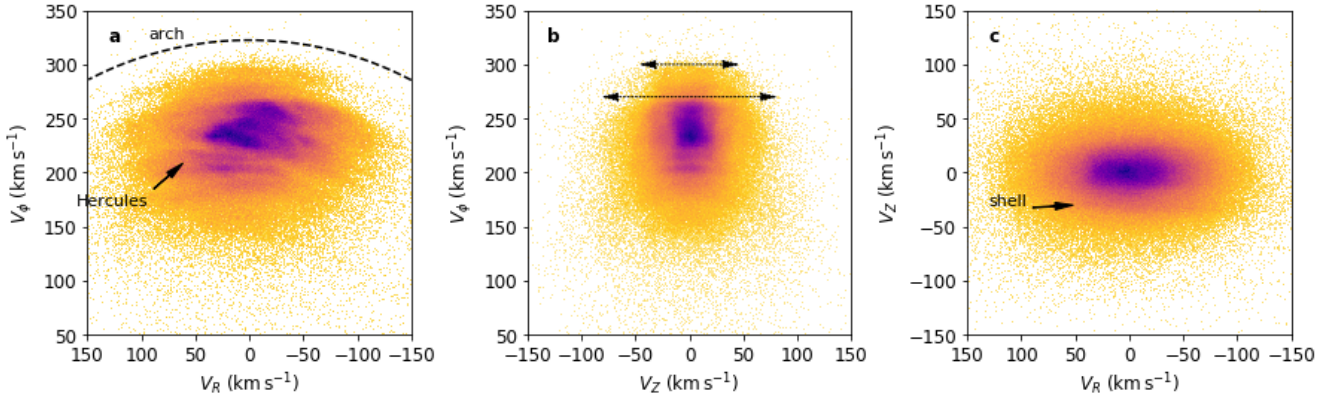


Figure 1. Distribution of velocities in the solar Galactocentric radius from Gaia DR2 data.

Two-dimensional histograms of radial, azimuthal and vertical Galactic cylindrical velocities for the stars in our sample located at $8.24 < R < 8.4$ kpc, in bins of 1 km s^{-1} width. V_R and V_ϕ are positive towards the Galactic anti-centre and the Galactic rotation direction, respectively. Although the bimodality seen in the leftmost panel, separating Hercules stream from the rest of the distribution was known, the numerous arches in this panel and the shell-like features especially involving the V_Z velocities are a new phenomenon revealed by *Gaia*.

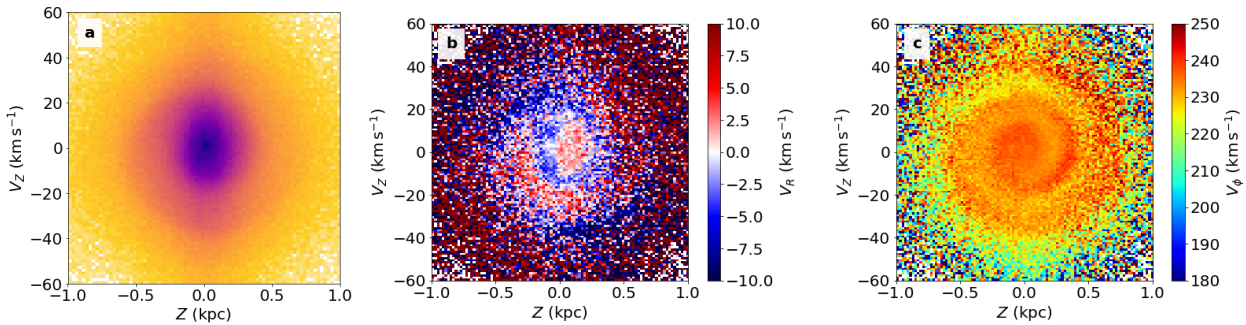


Figure 2. Distribution of stars in the vertical position-velocity plane $Z-V_Z$ for stars selected as in Fig. 1. a) Two-dimensional histogram in bins of $\Delta Z = 0.01$ kpc and $\Delta V_Z = 0.1 \text{ km s}^{-1}$; b) $Z-V_Z$ plane coloured as a function of median V_R in bins of $\Delta Z = 0.02$ kpc and $\Delta V_Z = 1 \text{ km s}^{-1}$; c) Same as b) but for V_ϕ .

Gaia is a cornerstone mission of the European Space Agency (ESA) that has been designed primarily to investigate the origin, evolution and structure of the Milky Way. *Gaia* has just delivered an exquisite product: the largest and most precise census of positions, velocities and other stellar properties for more than a billion stars. Here we explore the phase space of more than 6 million stars (positions and velocities) in the disk of the Galaxy in the first kiloparsecs around the Sun from the *Gaia* Data Release 2 (DR2, see Methods). We find that this phase space shows plenty of substructures which, especially in certain phase space projections, have never been seen before.

For decades, the vicinity of the Sun (~ 200 pc) has been the only region in the Galaxy with accurate position and velocity information. The velocity distributions known thus far contained substructure^{4–7},

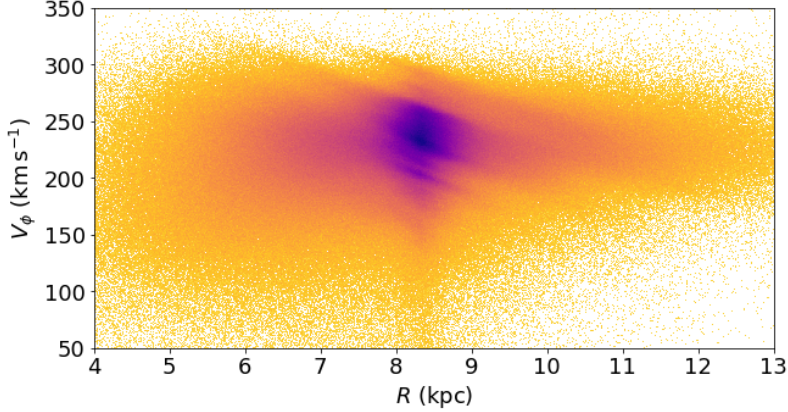


Figure 3. Distribution of azimuthal velocities as a function of Galactocentric radius throughout the Milky Way disk from Gaia DR2 data. Two-dimensional histogram for all observed stars in our sample with 6D phase space coordinates in bins of $\Delta V_\phi = 1 \text{ km s}^{-1}$, and $\Delta R = 0.01 \text{ kpc}$

especially in the V_R - V_ϕ plane in the form of roundish clumps and a bimodality^{5,8-10}. Now, the *Gaia* data uncovers a different view of this local velocity space that has remained blurred until now due to the limitations on the number of stars and the precision of the previously available datasets. From the selection of 935,590 stars located near the Solar Galactocentric radius (that is with radius $8.24 < R < 8.44 \text{ kpc}$ and covering an azimuthal angle of about 8°), we see that the distribution in the V_R - V_ϕ plane (Fig. 1a) is full of thin arches¹¹ many of which appear to have nearly constant kinetic energy in the plane, $E_k = \frac{1}{2}(V_R^2 + V_\phi^2)$.

Previously unidentified substructure is also present in other projections of velocity space. Arches are seen in V_ϕ - V_Z space (Fig. 1b), where the distribution of stars clearly does not follow a Gaussian or Schwarzschild distribution, but has a rather boxy appearance, and where the extent of the arches in V_Z , varies with their V_ϕ (arrows in Fig. 1b). Also the V_R - V_Z projection is boxy and depicts a few outstanding horizontal folds or shells, especially at $V_Z \sim -30 \text{ km s}^{-1}$ and $V_Z \sim 25 \text{ km s}^{-1}$.

The spatial coverage, high sampling and unprecedented precision of *Gaia* data allow us to also examine these substructures in projections now involving the spatial coordinates. Fig. 2a shows the projection of phase space in the vertical position and velocity Z - V_Z . The stars follow an impressive curled spiral-shaped distribution whose density increases towards the leading edge of the spiral. This “snail shell” pattern is responsible for the horizontal shells seen in Fig. 1c.

Fig. 2b and Fig. 2c show that the spiral shape is still present when the stars are colour-coded according to their V_R and V_ϕ values, implying a strong correlation between the vertical and in-plane motions of the stars. The pattern is particularly pronounced in the V_ϕ colour-coded case (Fig. 2c) even up to $V_Z \sim 40 \text{ km s}^{-1}$. Furthermore, we see a gradient in V_ϕ , with the larger velocities located at the leading part of the spiral shape, where the density of stars is also larger. It is the correlation between the spiral shape and the V_ϕ velocities that is likely creating the boxy structure seen in the V_ϕ - V_Z projection (Fig. 1b).

The distribution of azimuthal velocity V_ϕ versus cylindric radius R (Fig. 3) for all the 6,376,803 stars in our whole sample has a remarkable appearance showing a plethora of diagonal ridges. Each ridge in V_ϕ corresponds to an arch in the velocity space projection V_R - V_ϕ at the solar radius shown in Fig. 1a. However, Fig. 3 reveals that the arched structures are present at many different radii and that their characteristics vary with distance from the Galactic centre, diminishing their velocity towards the outskirts of the Galaxy in a continuous way.

The spiral shape of Fig. 2a is clearly reminiscent of the effects of phase mixing in two-dimensions

discussed in many areas of Astrophysics^{12–15} and also in quantum physics¹⁶. In realistic models of the Galaxy, disk stars follow orbits whose vertical oscillations have frequencies that depend on their orbital radius and on the vertical amplitude (see Methods). In the Z - V_Z plane, an ensemble of stars with slightly different frequencies will stretch out in phase space causing a spiral shape. As time goes by, this gets more tightly wound, and eventually, this process of phase mixing leads to a spiral that is so wound that the coarse-grained distribution appears to be smooth. The clarity of the spiral shape in the Z - V_Z plane revealed by the *Gaia* DR2 data, implies that this time has not yet arrived and thus provides unique evidence that phase mixing is currently taking place in the disk of the Galaxy.

This interpretation also implies that the shape of the spiral can be used to obtain information on: i) the shape of the potential, which determines the vertical frequencies, ii) the starting time of the phase mixing, and iii) the type of perturbation that brought the disk to a non-equilibrium state, which sets the initial conditions for the phase mixing event we are witnessing. By assuming a potential for the Milky Way, we estimated that the vertical phase mixing event started about 500 Myr ago, with an uncertainty range of [300, 900 Myr]. A toy model that illustrates this process is shown in Fig. 4a, which depicts a spiral shape similar to the data formed from an ensemble of stars with a starting distribution that is out of equilibrium (see Methods).

A possible perturbation that might have sparked the observed on-going vertical phase mixing is the influence of a satellite galaxy. In particular, the last pericentre of the orbit of the Sagittarius dwarf galaxy has been shown to have strong effects on the stellar disk^{17–19}. In addition, most models locate this event between 200 and 1000 Myr ago^{19–21}, which is fully consistent with our findings. Nevertheless, other processes that may induce snail shells could be the formation of the central bar and of transient spiral structure and other global changes in the potential, or the dissolution of a massive stellar system such as a cluster or accreted satellite.

The diagonal ridges in the azimuthal velocity as a function of Galactocentric radius (Fig. 3) could be signatures of phase mixing as well, now in the horizontal direction: each diagonal ridge would correspond to a successive wrap in phase space. Phase mixing processes have been shown to generate arches in the velocity space associated to motions in the plane V_ϕ - V_R ^{18, 22, 23}, which we now know are just projections of the diagonal ridges but at a fixed Galactic position. A simple toy model of phase mixing currently at work (Fig. 4b) shows also plenty of diagonal ridges in the R - V_ϕ plane. The V_ϕ velocity separation of consecutive ridges in the data is about 10 km s^{-1} , which is smaller than the separation in V_Z of successive turns of the spiral. Based on this and taking into account that the horizontal frequencies are smaller than the vertical ones, we can conclude that if these ridges are caused by a single perturbation, this should have taken place a longer time ago than that giving rise to the vertical mixing. Another possibility is that there were several perturbations creating superposed phase mixing features.

The bar and the spiral arms could potentially also induce diagonal ridges. Such non-axisymmetries have been long known to have a strong impact on disk dynamics in the plane^{24–27}. Indeed, a disk simulation with a Galactic potential containing a bar (Fig. 4c) and also other models²⁸ present similar substructures. These are created by the resonant orbital structure of the potential, which exhibit regions in phase space with stable and unstable orbits, and hence with over-densities and gaps.

To conclude, the *Gaia* data show strong signs of ongoing phase mixing out of a non-equilibrium state and of non-axisymmetries, both playing an important role in the dynamics of disk stars. Further detailed investigations on the phase space distribution of disk stars and their subsequent modelling should provide definitive answers about the history and structure of our Galaxy. On the other hand, the *Gaia* data also unequivocally evidence that some of the standard assumptions in Galactic dynamics, namely that our Galaxy is axisymmetric and in equilibrium, cannot really be blindly applied anymore.

H.D. Curtis was the righteous winner in the Great Debate claiming that the far nebulae observed

from the Earth were indeed galaxies like our own²⁹, or “island universes”. In the recent years, the concept of galaxies as isolated stellar systems has proved to be undoubtedly misleading. Grounds for the interaction between “island universes” come from the images of interactions between external galaxies³⁰ and the streams in the halo of the Milky Way³¹. More recently, it has been suggested that the disk of the Galaxy itself may have suffered from the impact of satellites which left an imprint in the form of velocity gradients, density asymmetries with respect to the mid-plane and planar rings^{17,32}. We have here provided the clearest evidence that our own Galaxy disk has suffered from perturbations bringing it to an out of equilibrium state, which may well be due to the interaction with an external satellite galaxy.

The promise of the so-called galactoseismology³³ has been to unveil the history of accretion and the characteristics of the satellite galaxies. Our findings provide additional means for this emergent research field and, moreover, they are the best evidence that galactoseismology is no longer a future promise but already a starting reality.

Acknowledgements

This work has made use of data from the European Space Agency (ESA) mission *Gaia* (<https://www.cosmos.esa.int/gaia>), processed by the *Gaia* Data Processing and Analysis Consortium (DPAC, <https://www.cosmos.esa.int/web/gaia/dpac/consortium>). Funding for the DPAC has been provided by national institutions, in particular the institutions participating in the *Gaia* Multilateral Agreement. This project has received funding from the European Union’s Horizon 2020 research and innovation programme under the Marie Skłodowska-Curie grant agreement No. 745617. This work was supported by the MDM-2014-0369 of ICCUB (Unidad de Excelencia ‘María de Maeztu’) and the European Community’s Seventh Framework Programme (FP7/2007-2013) under grant agreement GENIUS FP7 - 606740. AH gratefully acknowledges financial support from a VICI grant from the Netherlands Organisation for Scientific Research, NWO.

Additional information

Methods

Data and samples selection

We used Gaia sources for which the 6D phase space coordinates can be computed, that is all sources with available 5 parameters astrometric solution (sky positions, parallax and proper motions) and radial velocities. We selected only stars with positive parallaxes ϖ with relative uncertainty smaller than 20%, i.e. the ones satisfying $\varpi/\sigma_\varpi > 5$. This selection is to ensure that $1/\varpi$ is a reasonably good estimator of the distance to the stars³⁴. This sample has 6,376,803 stars and it has been well studied and characterised elsewhere¹¹. The data was obtained directly through the following query in the public Gaia Archive (<https://gea.esac.esa.int/archive/>):

```
SELECT G.source_id, G.radial_velocity, G.radial_velocity_error,
G.ra, G.ra_error, G.dec, G.dec_error, G.parallax, G.parallax_error,
G.pmra, G.pmra_error, G.pmdec, G.pmdec_error,
G.ra_dec_corr, G.ra_parallax_corr, G.ra_pmra_corr, G.ra_pmdec_corr,
G.dec_parallax_corr, G.dec_pmra_corr, G.dec_pmdec_corr,
G.parallax_pmra_corr, G.parallax_pmdec_corr, G.pmra_pmdec_corr
FROM gaiadr2.gaia_source G
WHERE G.radial_velocity IS NOT Null AND G.parallax_over_error>5.
AND G.parallax IS NOT Null
```

From the 5 parameter astrometric solution and line-of-sight velocities ($\alpha, \delta, \varpi, \mu_\alpha^*, \mu_\delta, V_{los}$) of these stars, we derived distances (as $1/\varpi$), positions and velocities in the cylindrical Galactic reference frame, that is ($R, \phi, Z, V_R, V_\phi, V_Z$). For convenience, we took ϕ positive in the direction of Galactic rotation and with origin at the line Sun-Galactic Centre. For these transformations, we adopted a vertical distance of the Sun above the plane of³⁵ 27 pc, a distance of the Sun to the Galactic centre³⁶ R_\odot of 8.34 kpc and a circular velocity at the Sun radius of³⁶ $V_{c,\odot} = 240 \text{ km s}^{-1}$. We assumed a peculiar velocity of the Sun with respect of the Local Standard of Rest of³⁷ $(U_\odot, V_\odot, W_\odot) = (11.1, 12.24, 7.25) \text{ km s}^{-1}$. Our choice of values gives $(V_{c,\odot} + V_\odot)/R_\odot = 30.2 \text{ km s}^{-1} \text{ kpc}^{-1}$ which is compatible with the reflex motion of Sgr A*³⁸. To derive the uncertainties in these coordinates, we propagate the full covariance matrix. The median errors in the V_R, V_ϕ, V_Z velocities are 1.4, 1.5, and 1.0 km s^{-1} , respectively, and 80% of stars have errors smaller than 3.3, 3.7, 2.2 km s^{-1} in these velocities. The positions in the Cartesian coordinates X - Y and X - Z are shown in Extended Data Fig. 5.

For part of our study, we selected from our sample the 935,590 stars located in the solar Galactic cylindrical ring, that is with Galactocentric radius $8.24 < R < 8.44 \text{ kpc}$ (dotted lines in Extended Data Fig. 5). For this selection, the median errors in the V_R, V_ϕ, V_Z velocities are 0.5, 0.8, and 0.6 km s^{-1} , respectively, and 80% of stars have errors smaller than $1.1, 2.0, 1.3 \text{ km s}^{-1}$ in these velocities.

We note that the velocity uncertainties are significantly smaller than the sizes of the substructures detected and that, together with the number of stars in our samples, this is what made possible their detection. Although there are some correlations between the astrometric Gaia observables³⁹, these are not responsible for the correlations and substructure seen in our phase space plots. This is because the stars in our sample are distributed through all sky directions, and the phase space coordinates of our sample come from combinations of astrometric measurements and radial velocities, in different contributions depending on the direction on the sky. Besides, the astrometric correlations for our sample are small (smaller than 0.2 in their absolute value for more than 50% of stars in our sample) and this, combined with the small errors, makes their contribution nonsignificant.

Models for the vertical phase mixing

We first reproduced the spiral shape observed in the Gaia DR2 data by using a simple toy model. Often the classic harmonic oscillator is employed to describe the vertical movement of stars in galaxy disks under the epicyclic theory². However, in these approximation, which is valid only for very small amplitude orbits for which the potential changes little vertically, stars have the same vertical oscillatory frequency v and there is no phase mixing. Instead, we used an anharmonic oscillator with potential of the shape $\Phi(Z) \propto -\alpha_0 + \frac{1}{2}\alpha_1 Z^2 - \frac{1}{4}\alpha_2 Z^4$. We took the coefficients $\alpha_1, \alpha_2, \alpha_3$ corresponding to the expansion for small Z of a Miyamoto-Nagai potential⁴⁰ with values of $a = 6.5 \text{ kpc}$, $b = 0.26 \text{ kpc}$, $M = 10^{11} M_\odot$ derived elsewhere¹⁵. These coefficients depend on Galactocentric radius R . In this anharmonic potential, the frequencies of oscillation depend on the amplitude of the oscillation A in the following way¹⁵:

$$v(A) = \alpha_1^{1/2} \left(1 - \frac{3\alpha_2 A^2}{8\alpha_1} \right), \quad (1)$$

Given an initial distribution of stars $Z(t=0)$ and $V_Z(t=0)$, the vertical amplitudes of the orbits can be derived through the conservation of energy and using the fact that at the vertical turn-around point of the orbit ($V_Z = 0$), the (vertical) kinetic energy is null¹⁵. Assuming that stars follow a simple harmonic oscillation (but with different frequencies), the movement of the stars with time is described by

$$Z = A \cos(v(A)t + \phi_0), \quad V_Z = -Av(A) \sin(v(A)t + \phi_0), \quad (2)$$

where the initial phase of the stars $\phi_0 \equiv \phi(t = 0)$ is obtained from the initial distribution of Z and V_Z and the corresponding amplitudes.

The phase space evolution described above is shown in the top row of Extended Data Fig. 6. Initially, the particles followed a Gaussian distribution in $Z(t = 0)$ and in $V_Z(t = 0)$ with mean and dispersion of -0.1 kpc and 0.04 kpc , and -2 km s^{-1} and 1 km s^{-1} , respectively. We located all particles at the same Galactocentric radius $R = 8.5\text{ kpc}$, and thus, they all move under the same functional form of the vertical potential. The initial conditions are shown in Extended Data Fig. 6a, where we colour-coded the particles according to its period. Following Eq. (2), each star follows a clockwise rotation in the Z - V_Z plane. However, they do it at a different angular speed: stars with smaller period located at the closer distances from the mid-plane ($Z = 0$) revolve faster than those located at the largest distances from the mid-plane. The whole continuous range of frequencies is what creates, therefore, the spiral shape. Extended Data Fig. 6b shows the evolution of the system for three initial phases of the time evolution when the spiral shape begins to form. Extended Data Fig. 6c shows the spiral shape after 1000 Myr of evolution.

In the Gaia data, we do not see a thin spiral but a thick one, with many of the stars in the volume participating in it. A similar effect was reached with our toy model when we included particles at different radius for which the vertical potential changes and range of amplitudes and frequencies also change. In Extended Data Fig. 6 (bottom row) we let the same system evolve as in the top row but starting with initial radius following a skewed normal distribution, which creates a density decreasing with radius as in galaxy disks, with skewness of 10, location parameter of 8.4 kpc and scale parameter of 0.2 kpc . The spiral structure is now thickened similarly to the data, with higher density of stars at the leading edge of the spiral.

We can estimate the time t of the vertical phase mixing event from the separation between two consecutive spiral turns because these have phase separation of 2π , that is $(v_2 t + \phi_0)_2 - (v_1 t + \phi_0)_1 = 2\pi$, where 1 and 2 indicate two consecutive spiral turns of the spiral. Therefore, we have that

$$t = \frac{2\pi}{v_2 - v_1}, \quad (3)$$

where we have assumed that the initial phase is the same for 1 and 2.

To estimate the time of the phase mixing event from the spiral seen in the Gaia data (Extended Data Fig. 8) we hence need to locate two consecutive turns of the spiral and estimate their vertical frequencies from their amplitudes and mean radius. To determine two consecutive turns of the spiral, we focused on stars at the turn-around points ($V_Z = 0$) at the leading edges of the spiral. By visual inspection, we determined an approximate range of Z in which the leading edges are located in Extended Data Fig. 8a and b. The ranges are marked with vertical lines in these panels and listed, together with the middle value, in Table 1. For these turn-around points the amplitudes are simply $A = Z$. To estimate the mean orbital radius, we used Extended Data Fig. 8b where we show the same plane as in Extended Data Fig. 8a but colour coded as a function of median guiding radius, this was approximated as $R_g \sim \frac{V_\phi * R_\odot}{V_c(R_\odot)}$, where we have used the values of $R_\odot = 8.34\text{ kpc}$ and $V_c(R_\odot) = 240\text{ km s}^{-1}$ assumed in the coordinate transformation of the data. We see that in the turn-around points the average R_g is around 8.2 kpc . Small changes in this value do not change significantly our final determination of the time of the perturbation.

To estimate the vertical orbital frequencies of these turn-around points, we could not use the toy model presented above since the model is valid only for oscillations with small amplitude A , in particular smaller than the vertical scale b of the potential ($A \ll 0.26\text{ kpc}$). Therefore, we took the model of Allen & Santillan⁴¹ with updated parameters that fit current estimations such as for the Sun Galactocentric radius or the circular velocity curve⁴². We computed the vertical frequency numerically in a grid of different radius and vertical amplitudes by integrating orbits and measuring their vertical periods (Extended Data

Fig. ??a). The vertical frequency can change along the orbits for stars with large eccentricities in the horizontal direction, but here for simplicity we put all particles on circular orbits. We estimated the vertical frequency at each turn-around position directly by interpolating the numbers of Extended Data Fig. 7a using the estimated values for the amplitude and radius.

Finally, taking each pair of turning points, we obtained an estimation of the time since the perturbation using (3). As an example, the two turning points (amplitudes) of the left part of the spiral are located at -0.59 ± 9 and -0.23 ± 5 , respectively. These correspond to vertical frequencies of $0.058^{+0.002}_{-0.002}$ and $0.072^{+0.002}_{-0.002}$ rad Myr $^{-1}$ for $R_g = 8.2$ kpc, which corresponds to a time of 461^{+183}_{-105} Myr.

We repeated the same procedure for the second pair of consecutive turning points and also for the edges of the spiral at $Z = 0$ (mid-plane points), which have $V_Z = A_{VZ} \equiv Av$, estimating the frequencies by interpolating the values of Extended Data Fig. 7b. The mid-plane positions are marked as horizontal lines in Extended Data Fig. 8. All results are summarised in Table 1 and Table 2. The mean of the three time estimations is 510 Myr and the minimum and maximum times from the uncertainty ranges are 356 and 856 Myr. We note that these values are subject to several approximations, namely that we used the vertical frequencies of circular orbits and for an assumed Galactic potential model, we considered a unique guiding radius, and we took equal initial phases for the turn-around and mid-plane points.

We finally run a simulation by integrating 100000 test particle orbits in the updated Allen & Santillan model with initial vertical positions and velocities following Gaussian distributions centred at $Z = -0.4$ kpc and -5 km s $^{-1}$ and dispersions of 0.15 kpc and 2. km s $^{-1}$, respectively. Horizontally in the disk plane, they were distributed following a skewed normal in radius R with scale parameter of 0.8 kpc, location parameter of 8, skewness of 10, and all particles at an azimuthal angle $\phi = 0$. We simulated only circular orbits: the horizontal velocities were set to 0 for the radial component and to the circular velocity at the particle's radius for the azimuthal one. The particles were integrated forwards in time for 500 Myr as estimated from the data. We note that this is not meant to be a fit to the data since we have not explored all possible initial configurations that could lead to a similar spiral shape. We see, though, that an initial distribution asymmetric in Z with most particles located at positive or negative Z is required to obtain a single spiral instead of a symmetrical double one.

Models for the horizontal phase mixing

We used a simple toy model to reproduce the lines observed in the $V_\phi - R$ plane based on previously published models²³. We considered that stars move in radial epicycles with frequency ω_R depending on their energy E and angular momentum L_Z , which for large amplitude oscillations can be approximated based on the orbital properties of a circular orbit of the same energy E ⁴³:

$$\omega_R(E, L) \approx \frac{\kappa(E)}{1 + \frac{e^2}{4}(\gamma - 1)(\gamma - 2)}, \quad (4)$$

where $\kappa(E)$ is the epicyclic frequency for nearly circular orbits, e is the eccentricity of the orbit and $\gamma \equiv \frac{2\Omega}{\kappa}$, where Ω is the angular frequency of the circular orbit. We used power law potentials of the type:

$$\Phi(R) = V_{c,\odot}^2 \times \begin{cases} \ln \frac{R}{R_\odot} & \text{for } \beta = 0 \\ \frac{1}{2\beta} \left(\frac{R}{R_\odot} \right)^{2\beta} & \text{for } \beta \neq 0. \end{cases} \quad (5)$$

which on units implying $R_\odot = 1$ and $V_{c,\odot} = 1$ can be simplified to:

$$\Phi(R) = \begin{cases} \ln R & \text{for } \beta = 0 \\ \frac{1}{2\beta} (R)^{2\beta} & \text{for } \beta \neq 0. \end{cases} \quad (6)$$

For these potentials, the quantities of (4) can be computed following equations derived elsewhere⁴³.

Given a perturbation that has left an uneven distribution of epicyclic angle, the stars wrap in epicyclic angle with time according to their frequency ω_R , following $\theta = \theta_0 + \omega_R \Delta t$. One can build a weighting function $w(L, E)$ to simulate the wraps every 2π of the epicyclic angle²³:

$$w(L, E) = \frac{1}{2} (1 + \cos(\omega_R t)) \quad (7)$$

Since the angular momentum and the energy are related to the velocity of a star $V_\phi = L_Z/R$ and $V_\phi = \sqrt{E/0.5 - V_R^2}$, the weighting function can be computed for every point in the velocity distribution at the solar neighbourhood²³ but also, as we did here, for any region in the Galaxy and, in particular, for every point in the R - V_ϕ plane, taking $V_R = 0$.

Extended Data Fig. 9 shows the weighting function in the R - V_ϕ plane for three different values of the slope of the rotation curve β after 1000 Myr of evolution, where we have used $R_\odot = 8.34$ kpc and $V_{c,\odot} = 240$. km s^{-1} . These panels show patterns qualitatively similar to the one observed in the Gaia data. As expected, the separation and shape of the diagonal rodges depends on the potential, which determined the values of the frequencies.

Finally, we used a more sophisticated toy model in Fig. 4b built by integrating orbits in the Galactic potential of Allen & Santillan⁴¹ with updated parameters that fit current estimations such as for the Sun Galactocentric radius or the circular velocity curve⁴². We used as initial conditions a set of test particles distributed in Galactocentric radius according to a skewed normal distribution with skewness of 10, location parameter of 4 kpc and scale parameter of 6 kpc. The azimuthal angle was fixed at 0. For simplicity, all particles were put at the mid-plane with null vertical velocities. The radial and azimuthal velocities were initialised, respectively, following Gaussian distributions centred at 0 with dispersion of 40 km s^{-1} and centred at the circular velocity at the particular radius with a dispersion of 30 km s^{-1} . The particle orbits were integrated for 1000 Myr.

Model for the horizontal resonances

The model of Fig. 4c is from a test particle simulation of orbits integrated in a Galactic potential model including a bar⁴⁴. The axisymmetric part of the potential was the Allen & Santillan model⁴¹. The Galactic bar potential was built using Ferrers ellipsoids⁴⁵ oriented with its semi-major axes at 20° from the Sun-Galactic centre line, and its pattern speed was set to $50 \text{ km s}^{-1} \text{ kpc}^{-1}$, which corresponds to a period of about 120 Myr. The simulation consisted of 68 million test particles with an initial radial velocity dispersion of 30 km s^{-1} at the Solar radius. Their orbits were first integrated in the axisymmetric potential model for 10 Gyr until they were approximately fully phase mixed. Next, the bar potential was grown in $T_{\text{grow}} \equiv 4$ bar rotations. More details on the bar potential, initial conditions and integration procedure are specified elsewhere⁴⁴. Here we used the final conditions after T_{grow} (~ 500 Myr) and 8 additional bar rotations (~ 1000 Myr). From all the particles in the simulation, we used only the ones located in a range of 10° in azimuthal angle centred on the Sun, similar to the our data sample. This selection contains 2,009,791 particles.

Data availability statement

The datasets used and analysed for the current study are derived from the data available in the public Gaia Archive, [<https://gea.esac.esa.int/archive/>]. The datasets and toy models generated and/or analysed are available from the corresponding author on reasonable request.

Extended Data

Extended Data Figures

Extended Data Tables

Z (kpc)	v (rad/Myr)	Time (Myr)
-0.59 ± 5	$0.058^{+0.002}_{-0.002}$	461^{+183}_{-105}
-0.23 ± 5	$0.072^{+0.002}_{-0.002}$	
0.40 ± 5	$0.065^{+0.003}_{-0.003}$	
0.75 ± 5	$0.054^{+0.001}_{-0.001}$	566^{+290}_{-140}

Table 1. Time estimations from the turn-around points of the spiral. The first column indicates the vertical position of the turn-around point, which is equal to the amplitude of the orbits except for the sign, and the estimated uncertainty range. The following columns are the frequency corresponding to these amplitude, and the starting time the phase mixing process corresponding to each pair of consecutive spiral turns.

A_{V_Z} (km s $^{-1}$)	v (rad/Myr)	Time (Myr)
-37 ± 3	$0.066^{+0.002}_{-0.002}$	505^{+253}_{-132}
-19 ± 3	$0.079^{+0.002}_{-0.002}$	

Table 2. Time estimations from the turn-around points of the spiral. The first column indicates the vertical velocity at the mid-plain passages, which is equal to the velocity amplitude of the orbits except for the sign, and the estimated uncertainty range. The following columns are the frequency corresponding to these amplitude, and the starting time of the phase mixing process corresponding to the pair of consecutive spiral turns.

References

1. Oort, J. H. Observational evidence confirming Lindblad's hypothesis of a rotation of the galactic system. *Bull. Astron. Inst. Neth.* **3**, 275 (1927).
2. Binney, J. & Tremaine, S. *Galactic Dynamics: Second Edition* (Princeton University Press, 2008).
3. Gaia Collaboration, Brown, A. & et al. Gaia Data Release 2: Summary of the contents and survey properties. *A&A* (2018).
4. Eggen, O. J. Star Streams and Galactic Structure. *AJ* **112**, 1595 (1996). DOI 10.1086/118126.
5. Dehnen, W. The Distribution of Nearby Stars in Velocity Space Inferred from HIPPARCOS Data. *AJ* **115**, 2384–2396 (1998). DOI 10.1086/300364. [arXiv:astro-ph/9803110](https://arxiv.org/abs/astro-ph/9803110).
6. Skuljan, J., Hearnshaw, J. B. & Cottrell, P. L. Velocity distribution of stars in the solar neighbourhood. *MNRAS* **308**, 731–740 (1999). DOI 10.1046/j.1365-8711.1999.02736.x. [arXiv:astro-ph/9905002](https://arxiv.org/abs/astro-ph/9905002).
7. Antoja, T., Figueras, F., Fernández, D. & Torra, J. Origin and evolution of moving groups. I. Characterization in the observational kinematic-age-metallicity space. *A&A* **490**, 135–150 (2008). DOI 10.1051/0004-6361:200809519. [0809.0511](https://arxiv.org/abs/0809.0511).

8. Eggen, O. J. Stellar groups. II. The ζ Herculis, ε Indi and 61 Cygni groups of high-velocity stars. *MNRAS* **118**, 154 (1958).
9. Raboud, D., Grenon, M., Martinet, L., Fux, R. & Udry, S. Evidence for a signature of the galactic bar in the solar neighbourhood. *A&A* **335**, L61–L64 (1998). [arXiv:astro-ph/9802266](https://arxiv.org/abs/astro-ph/9802266).
10. Antoja, T. *et al.* Constraints on the Galactic bar from the Hercules stream as traced with RAVE across the Galaxy. *A&A* **563**, A60 (2014). DOI 10.1051/0004-6361/201322623. [1309.4272](https://arxiv.org/abs/1309.4272).
11. Katz, D. & *et al.* Gaia Data Release 2: Mapping the Milky Way kinematic and large scale structure. *A&A* (2018).
12. Tremaine, S. The geometry of phase mixing. *MNRAS* **307**, 877–883 (1999). DOI 10.1046/j.1365-8711.1999.02690.x. [astro-ph/9812146](https://arxiv.org/abs/astro-ph/9812146).
13. Afshordi, N., Mohayaee, R. & Bertschinger, E. Hierarchical Phase Space Structure of Dark Matter Haloes: Tidal debris, Caustics, and Dark Matter annihilation. *Phys. Rev. D*, vol. 79, Issue 8, id. 083526 **79** (2008). URL <http://arxiv.org/abs/0811.1582> <http://arxiv.org/abs/0811.1582>. DOI 10.1103/PhysRevD.79.083526. [0811.1582](https://arxiv.org/abs/0811.1582).
14. Abel, T., Hahn, O. & Kaehler, R. Tracing the Dark Matter Sheet in Phase Space. *Mon. Notices Royal Astron. Soc. Vol. 427, Issue 1, pp. 61-76.* **427**, 61–76 (2011). URL <http://arxiv.org/abs/1111.3944>. DOI 10.1111/j.1365-2966.2012.21754.x. [1111.3944](https://arxiv.org/abs/1111.3944).
15. Candlish, G. N. *et al.* Phase mixing due to the Galactic potential: steps in the position and velocity distributions of popped star clusters. *Mon. Notices Royal Astron. Soc. Vol. 437, Issue 4, p.3702-3717* **437**, 3702–3717 (2013). URL <http://arxiv.org/abs/1311.1507>. DOI 10.1093/mnras/stt2166. [1311.1507](https://arxiv.org/abs/1311.1507).
16. Manfredi, G. & R. Feix, M. Theory and simulation of classical and quantum echoes. *Phys. review. E, Stat. physics, plasmas, fluids, related interdisciplinary topics* **53**, 6460–6470 (1996).
17. Purcell, C. W., Bullock, J. S., Tollerud, E. J., Rocha, M. & Chakrabarti, S. The Sagittarius impact as an architect of spirality and outer rings in the Milky Way. *Nat.* **477**, 301–303 (2011). DOI 10.1038/nature10417. [1109.2918](https://arxiv.org/abs/1109.2918).
18. Gómez, F. A., Minchev, I., Villalobos, Á., O’Shea, B. W. & Williams, M. E. K. Signatures of minor mergers in Milky Way like disc kinematics: ringing revisited. *MNRAS* **419**, 2163–2172 (2012). DOI 10.1111/j.1365-2966.2011.19867.x. [1105.4231](https://arxiv.org/abs/1105.4231).
19. de la Vega, A., Quillen, A. C., Carlin, J. L., Chakrabarti, S. & D’Onghia, E. Phase wrapping of epicyclic perturbations in the Wobbly Galaxy. *MNRAS* **454**, 933–945 (2015). DOI 10.1093/mnras/stv2055. [1507.07489](https://arxiv.org/abs/1507.07489).
20. Law, D. R. & Majewski, S. R. The Sagittarius Dwarf Galaxy: A Model for Evolution in a Triaxial Milky Way Halo. *ApJ* **714**, 229–254 (2010). DOI 10.1088/0004-637X/714/1/229. [1003.1132](https://arxiv.org/abs/1003.1132).
21. Laporte, C. F. P., Johnston, K. V., Gómez, F. A., Garavito-Camargo, N. & Besla, G. The Influence of Sagittarius and the Large Magellanic Cloud on the Milky Way Galaxy. *ArXiv e-prints* (2017). [1710.02538](https://arxiv.org/abs/1710.02538).
22. Fux, R. Order and chaos in the local disc stellar kinematics induced by the Galactic bar. *A&A* **373**, 511–535 (2001). DOI 10.1051/0004-6361:20010561. [arXiv:astro-ph/0105398](https://arxiv.org/abs/astro-ph/0105398).
23. Minchev, I. *et al.* Is the Milky Way ringing? The hunt for high-velocity streams. *MNRAS* **396**, L56–L60 (2009). DOI 10.1111/j.1745-3933.2009.00661.x. [0902.1531](https://arxiv.org/abs/0902.1531).

24. Contopoulos, G. & Grosbol, P. Stellar dynamics of spiral galaxies - Nonlinear effects at the 4/1 resonance. *A&A* **155**, 11–23 (1986).
25. Dehnen, W. The Effect of the Outer Lindblad Resonance of the Galactic Bar on the Local Stellar Velocity Distribution. *AJ* **119**, 800–812 (2000). DOI 10.1086/301226. [arXiv:astro-ph/9911161](https://arxiv.org/abs/astro-ph/9911161).
26. Quillen, A. C. & Minchev, I. The Effect of Spiral Structure on the Stellar Velocity Distribution in the Solar Neighborhood. *AJ* **130**, 576–585 (2005). DOI 10.1086/430885. [arXiv:astro-ph/0502205](https://arxiv.org/abs/astro-ph/0502205).
27. Antoja, T. *et al.* Stellar Kinematic Constraints on Galactic Structure Models Revisited: Bar and Spiral Arm Resonances. *ApJ* **700**, L78–L82 (2009). DOI 10.1088/0004-637X/700/2/L78. [0906.4682](https://arxiv.org/abs/0906.4682).
28. Michtchenko, T. A., Lépine, J. R. D., Barros, D. A. & Vieira, R. S. S. Combined dynamical effects of the bar and spiral arms in a Galaxy model. Application to the solar neighbourhood. *ArXiv e-prints* (2018). [1803.06995](https://arxiv.org/abs/1803.06995).
29. Hoskin, M. A. The 'Great Debate': What Really Happened. *J. for Hist. Astron.* **7**, 169 (1976).
30. Brastad, N. J. *et al.* The Spitzer Interacting Galaxies Survey: A Mid-infrared Atlas of Star Formation. *ApJS* **218**, 6 (2015). DOI 10.1088/0067-0049/218/1/6.
31. Belokurov, V. *et al.* The Field of Streams: Sagittarius and Its Siblings. *ApJ* **642**, L137–L140 (2006). DOI 10.1086/504797. [astro-ph/0605025](https://arxiv.org/abs/astro-ph/0605025).
32. Widrow, L. M., Barber, J., Chequers, M. H. & Cheng, E. Bending and breathing modes of the Galactic disc. *MNRAS* **440**, 1971–1981 (2014). DOI 10.1093/mnras/stu396. [1404.4069](https://arxiv.org/abs/1404.4069).
33. Widrow, L. M., Gardner, S., Yanny, B., Dodelson, S. & Chen, H.-Y. Galactoseismology: Discovery of Vertical Waves in the Galactic Disk. *ApJ* **750**, L41 (2012). DOI 10.1088/2041-8205/750/2/L41. [1203.6861](https://arxiv.org/abs/1203.6861).
34. Luri, X. & *et al.* Distances from parallaxes: on the proper use of astrometric data. *A&A* (2018).
35. Chen, B. *et al.* Stellar Population Studies with the SDSS. I. The Vertical Distribution of Stars in the Milky Way. *ApJ* **553**, 184–197 (2001). DOI 10.1086/320647.
36. Reid, M. J. *et al.* Trigonometric Parallaxes of High Mass Star Forming Regions: The Structure and Kinematics of the Milky Way. *ApJ* **783**, 130 (2014). DOI 10.1088/0004-637X/783/2/130. [1401.5377](https://arxiv.org/abs/1401.5377).
37. Schönrich, R. Galactic rotation and solar motion from stellar kinematics. *MNRAS* **427**, 274–287 (2012). DOI 10.1111/j.1365-2966.2012.21631.x. [1207.3079](https://arxiv.org/abs/1207.3079).
38. Reid, M. J. & Brunthaler, A. The Proper Motion of Sagittarius A*. II. The Mass of Sagittarius A*. *ApJ* **616**, 872–884 (2004). DOI 10.1086/424960. [arXiv:astro-ph/0408107](https://arxiv.org/abs/astro-ph/0408107).
39. Lindegren, L. & *et al.* Gaia Data Release 2: The astrometric solution. *A&A* (2018).
40. Miyamoto, M. & Nagai, R. Three-dimensional models for the distribution of mass in galaxies. *PASJ* **27**, 533–543 (1975).
41. Allen, C. & Santillan, A. An improved model of the galactic mass distribution for orbit computations. *Rev. Mexicana Astron. Astrofis.* **22**, 255–263 (1991).
42. Irrgang, A., Wilcox, B., Tucker, E. & Schiefelbein, L. Milky Way mass models for orbit calculations. *A&A* **549**, A137 (2013). DOI 10.1051/0004-6361/201220540. [1211.4353](https://arxiv.org/abs/1211.4353).

43. Dehnen, W. Approximating Stellar Orbits: Improving on Epicycle Theory. *AJ* **118**, 1190–1200 (1999). DOI 10.1086/301009. [astro-ph/9906081](https://arxiv.org/abs/astro-ph/9906081).
44. Romero-Gómez, M., Figueras, F., Antoja, T., Abedi, H. & Aguilar, L. The analysis of realistic stellar Gaia mock catalogues - I. Red clump stars as tracers of the central bar. *MNRAS* **447**, 218–233 (2015). DOI 10.1093/mnras/stu2457. [1411.6389](https://arxiv.org/abs/1411.6389).
45. Ferrers, N. On the potentials of ellipsoids, ellipsoidal shells, elliptic laminae and elliptic rings of variable densities. *QJ Pure Appl. Math* **14**, 1–22 (1877).

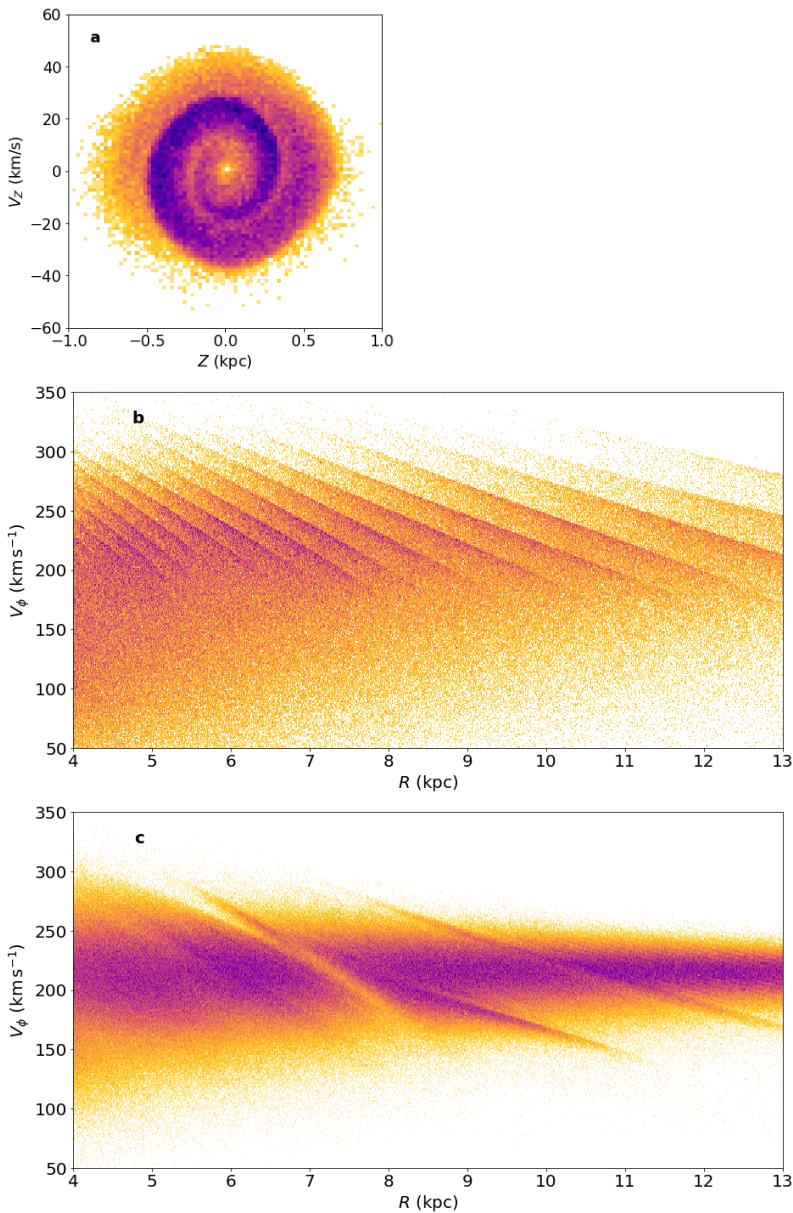


Figure 4. Models of the phase space distribution of the Galaxy disk. a) Modelled spiral shape created in the $Z-V_Z$ plane as the result of the phase mixing in the evolution of an ensemble of particles for 500 Myr in a Galactic potential, starting from a distribution that is out of equilibrium with the potential presumably after a certain perturbation (see Methods); b) Modelled diagonal ridges created in the $R-V_\phi$ plane as the result of the phase mixing in the evolution of an ensemble of particles for 1000 Myr in a Galactic potential, starting from a distribution that is out of equilibrium with the potential (see Methods); c) Modelled diagonal ridges created in the $R-V_\phi$ plane as the result of the effects of the barred potential and its resonant structure (see Methods).

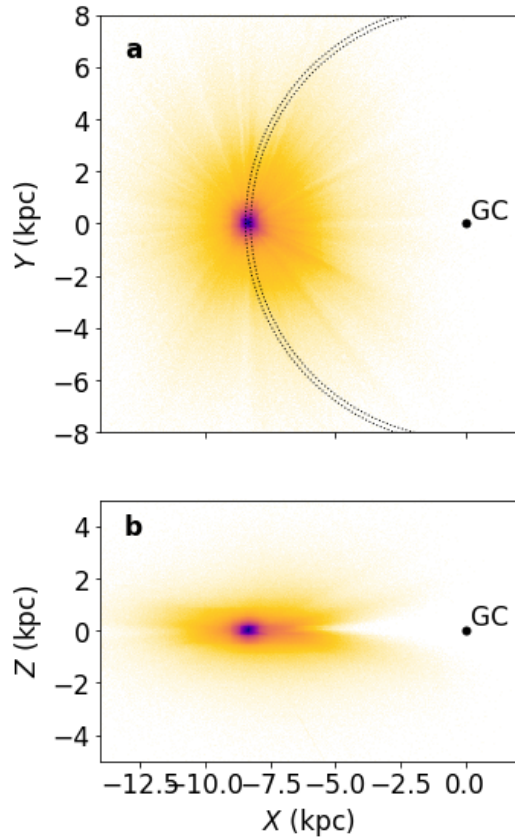


Figure 5. Distribution of stars in our sample in the disk of the Galaxy. Two dimensional histograms with bins of 0.05 kpc in the X - Y and X - Z projections. The dotted lines mark the selection of stars in the solar Galactic ring of between radius of $[8.24, 8.44]$ kpc. The Sun is located at $X = -8.34$ kpc and the Galactic Centre is marked with a black dot.

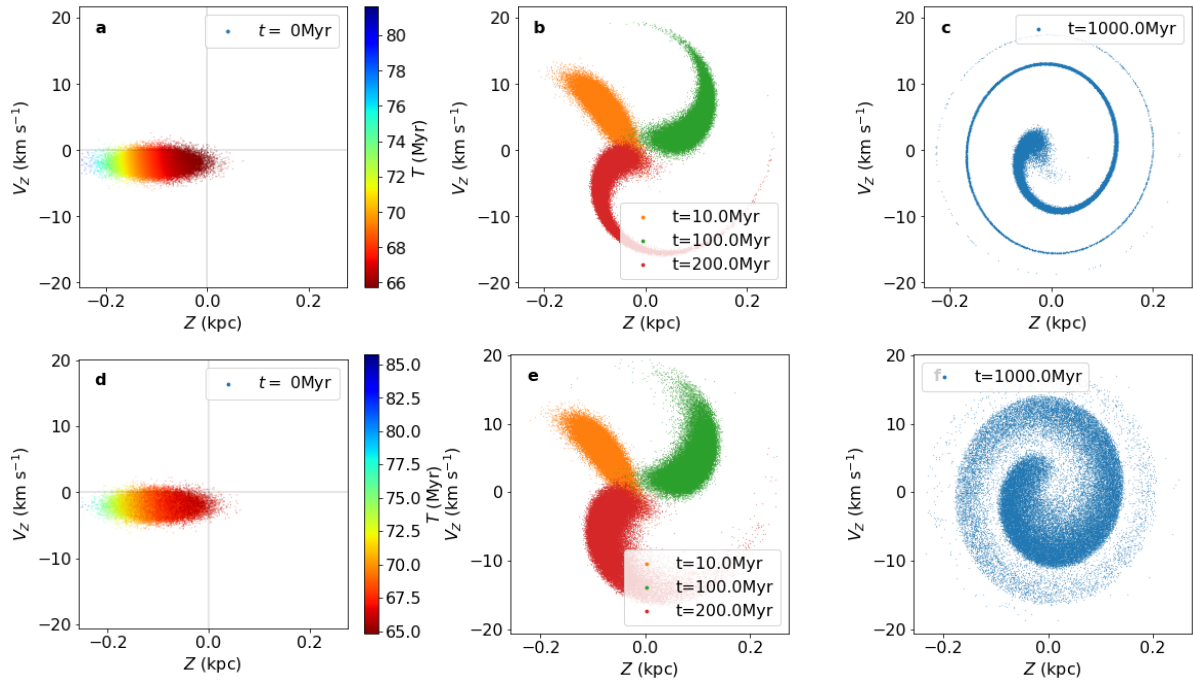


Figure 6. Spiral shape created in the phase space evolution under an anharmonic potential.

(a-b-c) phase space evolution for an ensemble of particles at a fixed Galactocentric radius of $R = 8.5$ kpc with an initial Gaussian distributions in $Z(t = 0)$ with mean of -0.1 kpc and dispersion of 0.04 kpc and in $V_Z(t = 0)$ with mean of -2 km s^{-1} and dispersion of 1 km s^{-1} . (d-e-f) Same as (a-b-c) but for an skewed normal distribution of initial radius with skewness of 10 , location parameter of 8.4 kpc and scale parameter of 0.2 kpc. In both rows, the evolution is the one of an anharmonic oscillator derived from the expansion of a Miyamoto-Nagai disk for small Z .

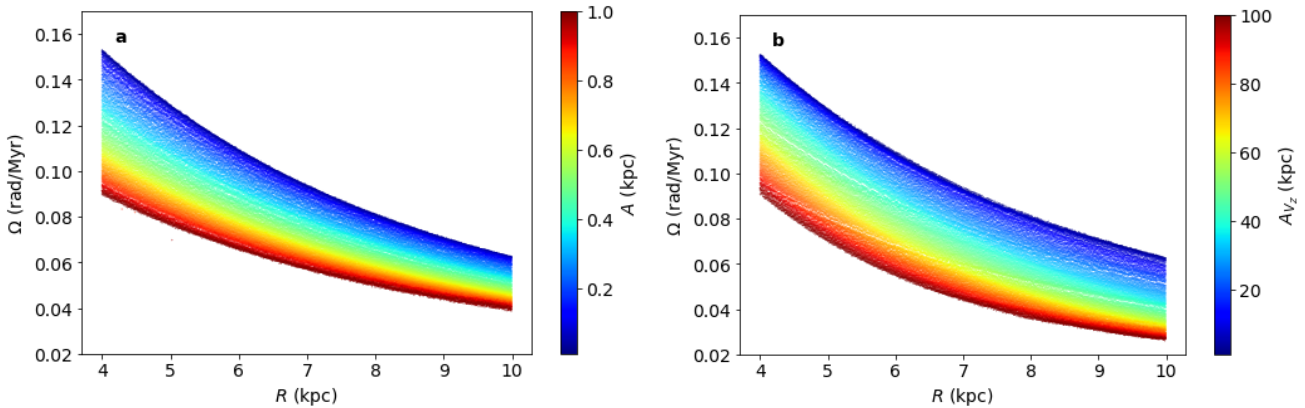


Figure 7. Vertical frequency for circular orbits in a Galaxy models potential. a) Frequencies a function of Galactocentric radius R and colour coded by vertical amplitude of the orbits. c) Frequencies a function of radius R and colour coded by vertical velocity amplitude of the orbits.

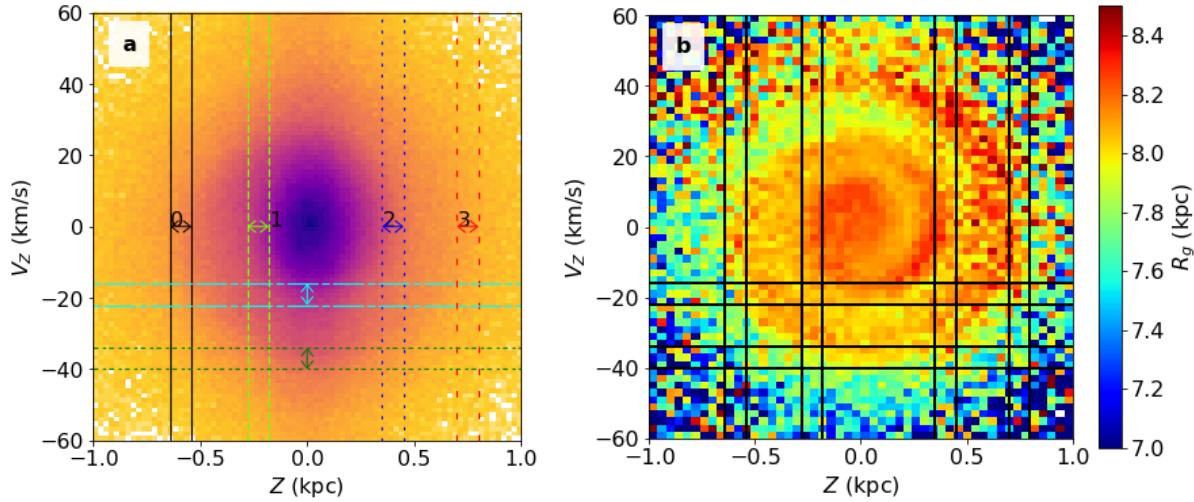


Figure 8. Position of the shells in the distribution of stars in the $Z - V_Z$ plane for stars at Galactic radius of [8.24,8.44] kpc. a) Two-dimensional histogram in bins of $\Delta Z = 0.01$ (kpc) and $\Delta V_Z = 0.1$ km s $^{-1}$ with horizontal and vertical lines showing the approximate locations of the observed shells; b) $Z - V_Z$ plane coloured as a function of median guiding radius R_g in bins of $\Delta Z = 0.02$ (kpc) and $\Delta V_Z = 1$ km s $^{-1}$.

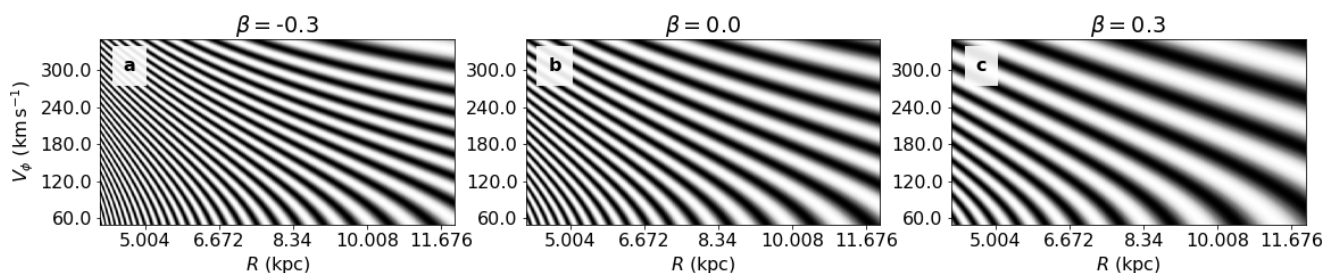


Figure 9. Ridges in the velocity-position space $R - V_\phi$ formed during horizontal phase mixing.
The panels show a weighting function with black regions corresponding to higher densities. The phase mixing corresponds to a toy model with wrappings in the epicyclic angle for power-law potentials for different values of β , the parameter characterising the flatness of the circular velocity curve.